Primary solid lung cancerous nodules with different sizes: computed tomography features and their variations

Zhi-gang Chu
The First Affiliated Hospital of Chongqing Medical University
Yan Zhang
Chongqing Three Gorges Medical College
Wang-jia Li
The First Affiliated Hospital of Chongqing Medical University
Qi Li
The First Affiliated Hospital of Chongqing Medical University
Yi-neng Zheng
The First Affiliated Hospital of Chongqing Medical University
Fa-jin Lv (cyscitg@163.com)
The First Affiliated Hospital of Chongqing Medical University https://orcid.org/0000-0002-8431-0350

Research article

Keywords: solid pulmonary nodule; lung cancer; computed tomography

Posted Date: October 15th, 2019

DOI: https://doi.org/10.21203/rs.2.11173/v2

Version of Record: A version of this preprint was published on November 7th, 2019. See the published version at https://doi.org/10.1186/s12885-019-6274-0.

Abstract

Background: The computed tomography (CT) features of small solid lung cancers and their changing regularity as they grow have not been well studied. The purpose of this study was to analyze the CT features of solid lung cancerous nodules (SLCNs) with different sizes and their variations. Methods: Between February 2013 and April 2018, a consecutive cohort of 224 patients (225 nodules) with confirmed primary SLCNs was enrolled. The nodules were divided into four groups based on tumor diameter (A: diameter ≤ 1.0 cm, 35 lesions; B: 1.0 cm < diameter ≤ 1.5 cm, 60 lesions; C: 1.5 cm < diameter ≤ 2.0 cm, 63 lesions; and D: 2.0 cm < diameter ≤ 3.0 cm, 67 lesions). CT features of nodules within each group were summarized and compared. Results: Most nodules in different groups were located in upper lobes (groups A–D：50.8%–73.1%) and had a gap from the pleura (groups A–D：89.6%–100%). The main CT features of smaller (diameter ≤ 1 cm) and larger (diameter > 1 cm) nodules were significantly different. As nodule diameter increased, more lesions showed a regular shape, homogeneous density, clear but coarse tumor–lung interface, lobulation, spiculation, spinous protuberance, vascular convergence, pleural retraction, bronchial truncation, and beam-shaped opacity ($p < 0.05$ for all). The presence of halo sign in all groups was similar (17.5%–22.5%; $p > 0.05$). Conclusions: The CT features vary among SLCNs with different sizes. Understanding their changing regularity is helpful for identifying smaller suspicious malignant nodules and early determining their nature in follow-up.

Background

Lung cancer is the most common tumor type and leading cause of cancer-related mortality worldwide [1, 2]. Pulmonary nodules as one of the main performances of lung cancer, they have always been the key point of research. Based on their density features in computed tomography (CT) images, cancerous nodules can be generally divided into solid and subsolid nodules, each with significantly different morphological and pathological features [3]. Several studies have been conducted on the differential diagnosis of benign and malignant subsolid nodules [4-8] and solid ones [9-13]. Compared with subsolid lung cancerous nodules, solid ones have a worse prognosis because of their rapid growth [14-16] and earlier development of metastases [16-19]. Therefore, early identification of malignant solid nodules, particularly smaller ones, based on CT features, is of great value for their prognosis.

Among various CT features, spiculation, lobulation, vascular convergence, and pleural retraction have been associated with malignancy in lung cancer [6, 20-25]; therefore, they are helpful in differentiating benign from malignant nodules. However, these features are usually absent from smaller nodules, making their diagnosis challenging. Management of smaller nodules has mainly relied on clinical follow-up, using changes in nodule size to determine benignity or malignancy [26-28]. However, there is no systematic report on changes other than size, including shape, density, margins, interface, and internal characteristics; their clinical significance also remains unclear. Therefore, further investigating CT features associated with the changing regularity of solid lung cancerous nodules (SLCNs) with different sizes has a potential to greatly improve early detection of malignant nodules.

To date, no study has reported imaging features associated with the development of primary SLCNs. Therefore, the purpose of this study is to investigate and summarize CT manifestations and their differences based on the nodules size and to provide a reference for early and accurate identification of potentially malignant small nodules.

Methods

Patients

The present study enrolled patients with pathologically confirmed peripheral lung cancer between February 2013 and April 2018. All patients underwent chest CT examination before surgery. Inclusion criteria was met by patients with (1) lesions comprising nodules with ≤ 3 cm diameter; (2) chest CT scan and surgery interval of one month, and (3) lesions not treated with antitumor therapy before CT examination. Patients were excluded if their CT images had poor quality (5 cases) or lesions were metastatic lung cancers (14 cases). A total of 224 patients (225 lesions) were included in the study.

CT examinations

All patients were examined with a 64-slice spiral CT scanner (SOMATOM Definition Flash, Siemens, Germany) with the following settings: tube voltage, 140kVp; tube current calculated according to individuals' weight, height, and body mass index; rotation time, 0.5 s; pitch, 1.0; collimation, 0.6 mm; slice thickness and interval for axial images, 5 mm and 5 mm; reorganization interval, 1 mm. Upon CT examination, patients were put in the supine position with both hands near the head. Image acquisition was performed from the level of the thoracic inlet to inferior to the costophrenic angle. Images were obtained with mediastinal window (width, 400 HU; level, 30 HU) and lung window (width, 1500 HU; level, −600 HU) settings.

Image analysis

All patients' CT data were reviewed on a workstation (Advantage Workstation 4.6; GE Healthcare) by two senior chest radiologists who were blinded to the pathological results of lesions. Interpretation discrepancy, if any, was resolved by consensus.

The followings features were evaluated on CT images: lesion size (average of the maximal long-axis and perpendicular maximal short-axis dimension); distribution in different lobes (left superior and inferior lobes and right superior, middle, and inferior lobes); location (clinging to pleura or not); shape (regular: oval, round, and polygonal or irregular); internal features (calcification, air bronchogram, vacuole, cavity); density (homogenous or heterogeneous); margins (lobulation, spiculation, spinous protuberance); and tumor–lung interface (coarse, unclear, or smooth). In addition, peripheral lesion areas were also evaluated, including vascular convergence, pleural retraction, bronchial truncation, and beam-shaped opacity. Pleural effusions and lymph nodes in the hilum and mediastinum were further evaluated.

Enlarged mediastinal and hilar lymph nodes were generally defined as diameter >1 cm in short axis on chest CT scans.

For investigating the differences in CT features of SLCNs with different sizes, especially for the smaller ones, nodules were divided into four groups according to tumor size: Group A: diameter ≤ 1.0 cm; Group B: 1.0 cm < diameter ≤ 1.5 cm; Group C: 1.5 cm < diameter ≤ 2.0 cm; and Group D: 2.0 cm < diameter ≤ 3.0 cm.

Statistical analysis

Clinical data and CT features of nodules were statistically analyzed for each group. Continuous variables were expressed as mean ± standard deviation, whereas categorical variables were expressed as absolute number and percentage. Independent sample *t*-tests were used to compare age among different groups. A chi-square test was used to compare differences in patients' clinical and pathological data, distribution and location of nodules, and various CT features among groups. Tukey-Kramer test was used for multiple comparisons between the groups. A *p*-value less than 0.05 was considered statistically significant. All statistical analyzes were performed through the statistical software SPSS (version 22.0 for Windows, SPSS Inc., Chicago, Illinois, USA).

Results

Patient Characteristics

Among the 224 patients, 129 (57.6%) were male and 95 (42.4%) were female. Patients were aged 38–83 years, with an average age of 61.7 ± 9.5 years. A total of 127 (56.7%) cases had cough, expectoration, hemoptysis, chest pain, or chest tightness. The number of SLCNs in groups A, B, C, and D was 35, 60, 63, and 67, respectively. **Table 1** summarizes clinical and pathological data of patients included in each group. No significant differences were found in gender, age, clinical symptoms, smoking history, and histopathological types of lung cancer among the four groups ($p > 0.05$).

Table 1. Patients' clinical and pathological data

	Group A (n=35)	Group B (n=60)	Group C (n=63)	Group D (n=67)	*p-value*
Age (years)	59.3 ± 9.2	63.0 ±10.6	60.9 ± 8.3	64.0 ± 9.0	0.841
Male	18 (51.4)	35 (58.3)	36 (57.1)	41 (61.2)	0.821
Smokers	12 (34.3)	20 (33.3)	29 (46.0)	34 (50.8)	0.157
Clinical symptoms	16 (45.7)	32 (53.3)	42 (66.7)	37 (55.2)	0.204
Pathological types					
Adenocarcinoma	32 (91.4)	55 (91.7)	51 (81.0)	56 (83.6)	0.245
Squamous cell carcinoma	1 (2.9)	5 (14.3)	10 (15.9)	6 (9.0)	0.191
Others	2 (5.7)	0 (0)	2 (3.2)	5 (7.5)	0.174

The data are expressed as n (%).

Lesion distribution and location

Nodules distribution and location are summarized in **Table 2**. In the four groups, nodules were mainly distributed in the upper lobes (50.8%–73.1%) and most did not cling to pleura (89.6%–100%).

Table 2. Distribution and location of nodules

	Group A (n=35)	Group B (n=60)	Group C (n=63)	Group D (n=67)	*p-value*
Right lung	28 (80.0)	33 (55.0)	31 (49.2)	42 (62.7)	0.022
SL	15 (42.9)	20 (33.3)	16 (25.4)	29 (43.3)	0.137
ML	5 (14.3)	2 (3.3)	4 (6.4)	5 (7.5)	0.252
IL	8 (22.9)	11 (18.3)	11 (17.5)	8 (11.9)	0.540
Left lung	7 (20)	27 (45)	32 (50.8)	25 (37.4)	0.022
SL	6 (17.1)	17 (28.3)	16 (25.4)	20 (29.9)	0.550
IL	1 (2.9)	10 (16.7)	16 (25.4)	5 (7.5)	0.005
SLs of both lungs	21 (60.0)	37 (61.7)	32 (50.8)	49 (73.1)	0.074
ILs of both lungs	9 (25.8)	21 (35)	27 (42.9)	13 (19.4)	0.026
Relationship with pleura					
Not clinging to pleura	35 (100.0)	58 (96.7)	58 (92.1)	60 (90)	0.114
Clinging to pleura	0 (-)	2 (3.33)	3 (4.76)	6 (8.96)	0.114

SL= Superior lobe, ML= Middle lobe, IL = Inferior lobe.

The data are expressed as n (%).

CT characteristics of lesions and their surroundings

Nodule CT features are summarized in **Table 3**. As nodule diameter increased, more lesions had regular shapes, homogeneous density, clear but coarse tumor-lung interface, lobulation, spiculation, spinous protuberance, vascular convergence, pleural retraction, bronchial truncation, and beam-shaped opacity ($p < 0.05$ for each) (**Figure 1-4**). However, the significant differences in various CT features were mainly detected between nodules in group A (diameter ≤ 1cm) and those in groups B, C and D (diameter > 1cm). Additionally, presence of halo sign in groups A and B was

Table 3. CT features of nodules in different size

CT features	Group A (n=35)	Group B (n=60)	Group C (n=63)	Group D (n=67)	*p-value*	Sig.
Shape						
Round	9 (25.7)	14 (23.3)	15 (23.8)	15 (22.4)	0.986	–
Oval	16 (45.7)	41 (68.3)	42 (66.7)	48 (71.6)	0.060	–
Polyonal	5 (14.3)	3 (5)	4 (6.3)	2 (3.0)	0.154	–
Irregular	5 (14.3)	2 (3.3)	2 (3.2)	2 (3.0)	0.049	A/BCD
Size (mm)	8.2±1.4	12.8±1.3	17.7±1.4	24.1±2.7	/	
Heterogeneous density	18 (51.4)	15 (25)	8 (12.7)	3 (4.5)	0.000	A/BCD
Internal feature						
Calcification	0 (-)	0 (-)	1 (1.6)	1 (1.5)	0.687	–
Vacuole	5 (14.3)	5 (14.3)	4 (6.4)	11 (16.4)	0.242	–
Air bronchogram	1 (2.9)	1 (1.7)	5 (7.9)	12 (17.9)	0.005	A/BCD
Cavity	0	1 (1.7)	7 (11.1)	4 (6.0)	0.051	–
Margin						
Lobulation	10 (28.6)	22 (36.7)	36 (57.1)	47 (70.1)	0.000	AB/CD
Spiculation or spinous protuberance	7 (20)	27 (45)	36 (57.1)	47 (70.1)	0.000	A/BCD
Halo sign	7 (20)	15 (25)	11 (17.5)	12 (17.9)	0.712	–
Tumor-lung interface						
Coarse	26 (74.3)	48 (80)	55 (87.3)	64 (95.5)	0.013	A/D
Unclear	6 (17.1)	7 (11.7)	3 (4.8)	1 (1.5)	0.016	A/D
Smooth	3 (8.6)	5 (14.3)	5 (7.9)	2 (3.0)	0.553	–
Bronchial truncation	0 (-)	8 (13.3)	10 (15.9)	18 (26.9)	0.005	A/BCD
Vascular convergence	6 (17.1)	32 (53.3)	43 (68.3)	50 (74.6)	0.000	A/BCD
Beam-shaped opacity	3 (8.6)	15 (25)	15 (23.8)	26 (38.8)	0.010	A/BCD
Pleural retraction	3 (8.6)	22 (36.7)	28 (44.4)	34 (50.8)	0.000	A/BCD
Obstructive pneumonia	0 (-)	1 (1.67)	4 (6.4)	5 (7.5)	/	/

The data are expressed as n (%). Heterogeneous density indicates the density of nodules in addition to calcification, vacuole, air bronchogram, and cavity. A/BCD indicates there is significant difference between group A and B but no significant difference among groups of B, C and D. AB/CD indicates there is significant difference between group B and C but no significant difference between group A and B or group C and D. A/D indicates there is significant difference only between group A and D.

CT characteristics of suspicious malignancy for group A nodules

Combining with lesion distribution, location, and morphological features, the main CT characteristics indicating suspicious malignancy for group A nodules were summarized in **table 4**.

Table 4. CT characteristics indicating suspicious malignancy for group A nodules

CT features	Numbers	Percentage (%)
SLs of both lungs†	21	60.0
Not clinging to pleura†	35	100.0
Irregular shape*	5	14.3
Heterogeneous density*	18	51.4
Lobulation‡	10	28.6
Spiculation or spinous protuberance‡	7	20
Coarse tumor-lung interface†	26	74.3
Unclear tumor-lung interface*	6	17.1
Halo sign†	7	20

SL= Superior lobe; † indicates the common features for group A-D nodules; * indicates these features are relatively common in group A nodules. ‡ indicates these features are relatively rare in group A nodules.

Lymph nodes in the hilum and mediastinum and pleural effusion

As nodule size increased, the incidence of enlarged lymph nodes in the hilum or mediastinum also gradually increased (8.6%, 18.3%, 27.0%, and 46.3% for each group; $p < 0.001$). Incidence of pleural effusion was extremely low for four groups.

Discussion

This study showed that the distribution of SLCNs in different size groups was similar. It was generally believed that the lung cancers were mainly distributed in the upper lobes [29-31]. Concerning nodule location, most nodules, particularly the smaller ones, were not connected with the adjacent pleura. It appeared that the space between the tumor and pleura will subsist until the nodules grow large enough to involve it [32]. It is possible that a SLCN is typically derived from the distal bronchus, and a distance exists between the lesion and pleura. These findings suggested that smaller nodules clinging to the pleura, which are usually detected on chest CT scan, were less likely to indicate lung cancer.

In this study, the smaller lesions (≤ 1cm) usually had different CT features with the bigger one (> 1cm). As nodule size increased, they acquired a more regular shape, and the margins and surrounding features also gradually increased. It may be because a nodule becomes more regular with an increase in size, and the limitation of the surrounding structure becomes more obvious. Lobulation, spiculation, pleural retraction, and vascular convergence are considered common signs of malignancy in lung cancer [6, 20-25]. However, for smaller nodules, traction and invasion of surrounding blood vessels and tissues, as well as tumor and peritumoral fibrosis were not obvious. As nodules increased, the invasiveness of the surrounding tissue also increased, and more signs were evident.

Siegelman et al. [33] reported that the incidence of coarse tumor–lung interface in lung cancer was significantly higher than that in benign lesions. In this study, tumor–lung interface in each group was mainly coarse. Additionally, the incidence of coarse interface increased with the increasing size of the nodule. This may be because tumor cells locally infiltrate the peripheral tissue, particularly the bigger nodules. However, the smaller the nodules, the higher the incidence of unclear interface, which may be

related to the relatively sparse tumor cells in the peripheral areas of nodules. Therefore, for smaller solid nodules with unclear interface, the possibility of lung cancer cannot be completely excluded; follow-up is recommended to avoid an erroneous diagnosis.

The growth of solid lung cancer is a gradual process. The tumor cells gradually accumulate, and the lesion size continuously increases. Theoretically, tumor density will be more homogeneous on plain CT scan with an increase in the lesion size. In the present study, smaller nodules had a higher incidence of heterogeneous density, particularly those less than 1 cm in diameter. However, incidence of internal calcification, vacuole sign, or cavity was low in each group, like the previous reports [34, 35]. Therefore, small solid nodules with heterogeneous density can be selectively observed, and lung cancer should be highly suspected once their density increases and becomes homogeneous.

Beam-shaped opacity is a banded ground glass opacity, which is located at the side of the tumor close to the pleura in different directions. It is common in adenocarcinoma and highly significant in the diagnosis of lung cancer [36]. This sign may be related to the traction of the surrounding lung tissue. In this study, the incidence of beam-shaped opacity was higher in the group D, but it was significantly lower in the group A. This implicates that small nodules are usually not able to cause significant changes in surrounding structures.

Halo sign was a nonspecific sign around solid pulmonary nodules, and its border was usually clear for lung cancer [37]. In this study, a well-defined halo sign was mainly located on one side of the nodule, and its incidence was slightly higher in smaller lesions. Therefore, the smaller solid nodules without other features but halo sign should be suspicious for lung cancer.

Overall, regarding the smaller pulmonary nodules, follow-up looks like a good way to discriminate their nature based on CT feature changes. Recent study confirmed that quantitative image features (“radiomics”) could also discriminate benign from malignant pulmonary nodules [38]. Additionally, quantitative radiomic signatures showed the potential to reveal and predict the tumor growth speed, and could identify the indolent from aggressive lung cancer [39]. Thus, radiomics may provide a new way for evaluating and managing indeterminate pulmonary nodules in the future.

This study had several limitations. Evaluation of CT feature changing regularity for SLCNs was performed by comparing grouped nodules with different sizes rather than only following one group of lesions. Thus, results obtained here should be confirmed in clinical practice. Additionally, pathological types of SLCNs varied but showed no significant differences among different groups. Therefore, present results seem to represent a general, rather than a specific tumor type. It should be noted that some types within smaller samples may not conform to the general morphological development.

Conclusions

SLCNs morphological changes presented some degree of regularity in their growth process. With diameter increasing, more nodules had regular shapes, homogeneous density, clear but coarse tumor-

lung interface, and margin or peripheral signs. Thus, larger nodules could be easily diagnosed due to presence of more features. However, for smaller nodules located in the upper lobe, not clinging to the pleura, showing irregular shape, heterogeneous density, unclear tumor–lung interface, or well-defined halo sign, malignancy should be suspected. Understanding the changing regularity of SLCNs is helpful for identifying smaller suspicious malignant nodules and early determining its nature in follow-up.

Abbreviations

CT: computed tomography

SLCN: solid lung cancerous nodule

Declarations

Acknowledgments

No.

Funding

This study was supported by the National Natural Science Foundation of China (81601545) and Chongqing Health and Family Planning Commission Foundation (2016MSXM018) of China. The funding was used to conduct all data analyses and cover publication fees. The funding bodies did not have any influence on the design of the study, collection, analysis, interpretation of data or in writing the manuscript.

Authors' contributions

Z.-G. C. and Y. Z. contributed to the data analysis and manuscript writing. W.-J. L., Q. L. and Y.-N. Z. were involved in performing data collection. F.-J. L. was responsible for the study coordination. All authors have read and approved the manuscript, and ensure that this is the case.

Ethics Approval and Consent to Participate

The Research Ethics Committee of The First Affiliated Hospital of Chongqing Medical University (IRB No. 2019-062) approved this study. All the participants provided written informed consent.

Consent for Publication

Not applicable.

Availability of Data and Material

Please contact author for data requests.

Competing Interests

The authors have declared that no competing interest exists.

References

1. Chen W, Zheng R, Baade PD, Zhang S, Zeng H, Bray F, et al. Cancer statistics in China, 2015, CA. Cancer J Clin. 2016; 66: 115-132.
2. Jemal A, Bray F, Center MM, Ferlay J, Ward E, Forman D. Global cancer statistics, CA. Cancer J Clin. 2011; 61: 69-90.
3. Naidich DP, Bankier AA, MacMahon H, Schaefer-Prokop CM, Pistolesi M, Goo JM, et al. Recommendations for the management of subsolid pulmonary nodules detected at CT: a statement from the Fleischner Society. Radiology. 2013; 266: 304-317.
4. Qiu ZX, Cheng Y, Liu D, Wang WY, Wu X, Wu WL, et al. Clinical, pathological, and radiological characteristics of solitary ground-glass opacity lung nodules on high-resolution computed tomography. Ther Clin Risk Manag. 2016; 12: 1445-1453.
5. Chung K, Jacobs C, Scholten ET, Goo JM, Prosch H, Sverzellati N et al. Lung-RADS category 4X: does it improve prediction of malignancy in subsolid nodules? Radiology. 2017; 284: 264–271.
6. Hu H, Wang Q, Tang H, Xiong L, Lin Q. Multi-slice computed tomography characteristics of solitary pulmonary ground-glass nodules: Differences between malignant and benign. Thorac Cancer. 2016; 7: 80-87.
7. Lee HY, Choi YL, Lee KS, Han J, Zo JI, Shim YM. et al. Pure ground-glass opacity neoplastic lung nodules: histopathology, imaging, and management. AJR. Am J Roentgenol. 2014; 202: 224-33.
8. Wu F, Tian SP, Jin X, Jing R, Yang YQ, Jin M et al. CT and histopathologic characteristics of lung adenocarcinoma with pure ground-glass nodules 10 mm or less in diameter. Eur Radiol. 2017; 27: 1-7.
9. Walter JE, Heuvelmans MA, Bock GH, Yousaf-Khan U, Groen HJM, Aalst CMV. et al. Characteristics of new solid nodules detected in incidence screening rounds of low-dose CT lung cancer screening: the NELSON study. Thorax. 2018; 73: 741-747.
10. Walter JE, Heuvelmans MA, de Jong PA, Vliegenthart R, van Ooijen PMA, Peters RB, et al. Occurrence and lung cancer probability of new solid nodules at incidence screening with low-dose CT: analysis of data from the randomised, controlled NELSON trial. Lancet Oncol. 2016; 17: 907-916.
11. Shinohara S, Hanagiri T, Takenaka M, Chikaishi Y, Oka S, Shimokawa, H, et al. Evaluation of undiagnosed solitary lung nodules according to the probability of malignancy in the American College of Chest Physicians (ACCP) evidence-based clinical practice guidelines. Radiol Oncol. 2014; 48: 50-55.
12. Sim YT, Poon FW. Imaging of solitary pulmonary nodule-a clinical review. Quant Imaging Med Surg. 2013; 3: 316-326.

13. Henschke CI, Yankelevitz DF, Reeves AP, Cham MD. Image analysis of small pulmonary nodules identified by computed tomography. Mt Sinai J Med. 2011; 78: 882-93.
14. Oda S, Awai K, Murao K, Ozawa A, Utsunomiya D, Yanaga Y, et al. Volume-doubling time of pulmonary nodules with ground glass opacity at multidetector CT: Assessment with computer aided three-dimensional volumetry. Acad Radiol. 2011; 18: 63-69.
15. Wang X, Han R, Guo F, Li X, Zheng W, Wang Q, et al. Analysis of Growth Curve Type in Pulmonary Nodules with Different Characteristics, Zhongguo Fei Ai Za Zhi. 2017; 20: 334-340.
16. Hasegawa M, Sone S, Takashima S, Li F, Yang ZG, Maruyama Y, et al. Growth rate of small lung cancers detected on mass CT screening. Br J Radiol. 2000; 73: 1252-1259.
17. Zhong W, Yang X, Bai J, Yang J, Manegold C, Wu Y. Complete mediastinal lymphadenectomy: the core component of the multidisciplinary therapy in resectable non-small cell lung cancer. Eur J Cardiothorac Surg. 2008; 34: 187-195.
18. Wolf AS, Richards WG, Jaklitsch MT, Gill R, Chirieac LR, Colson YL, et al. Lobectomy versus sublobar resection for small (2 cm or less) non-small cell lung cancers. Ann Thorac Surg. 2011; 92: 1819-1823.
19. Lee SM, Park CM, Paeng JC, Im HJ, Goo JM, Lee HJ, et al. Accuracy and predictive features of FDG-PET/CT and CT for diagnosis of lymph node metastasis of T1 non-small-cell lung cancer manifesting as a subsolid nodule. Eur Radiol. 2012; 22: 1556-1563.
20. Snoeckx A, Reyntiens P, Desbuquoit D, Spinhoven MJ, Van Schil PE, van Meerbeeck JP, et al. Evaluation of the solitary pulmonary nodule: size matters, but do not ignore the power of morphology. Insights Imaging. 2018; 9: 73-86.
21. Ost DE, Gould MK. Decision Making in Patients with Pulmonary Nodules. Am J Respir Crit Care Med. 2012; 185: 363-372.
22. Wang X, Lv L, Zheng Q, Huang X, Li B. Differential diagnostic value of 64 slice spiral computed tomographvy in solitary pulmonary nodule. Exp Ther Med. 2018; 15: 4703-4708.
23. Harders SW, Madsen HH, Rasmussen TR, Hager H, Rasmussen F. High resolution spiral CT for determining the malignant potential of solitary pulmonary nodules: refining and testing the test. Acta Radiol. 2011; 52: 401-409.
24. Miyamoto A, Kurosaki A, Fujii T, Kishi K, Homma S. HRCT features of surgically resected invasive mucinous adenocarcinoma associated with interstitial pneumonia. Respirology. 2017; 22: 735-743.
25. Oda S, Awai K, Liu D, Nakaura T, Yanaga Y, Nomori H, et al. Ground-Glass Opacities on Thin-Section Helical CT: Differentiation Between Bronchioloalveolar Carcinoma and Atypical Adenomatous Hyperplasia. Am J Roentgenol. 2012; 190: 1363-1368.
26. Gould MK, Donington J, Lynch WR, Mazzone PJ, Midthun DE, Naidich DP, et al. Evaluation of individuals with pulmonary nodules: when is it lung cancer? Diagnosis and management of lung cancer, 3rd ed: American College of Chest Physicians evidence-based clinical practice guidelines. Chest. 2013; 143: e93S-120S.

27. Patel VK, Naik SK, Naidich DP, Travis WD, Weingarten JA, Lazzaro R, et al. A practical algorithmic approach to the diagnosis and management of solitary pulmonary nodules: part 1: radiologic characteristics and imaging modalities. Chest. 2013; 143: 825-39.
28. Pinsky PF, Gierada DS, Nath PH, Munden R. Lung cancer risk associated with new solid nodules in the national lung screening trial. AJR. Am J Roentgenol. 2017; 209: 1-
29. Lindell RM, Hartman TE, Swensen SJ, Jett JR, Midthun DE, Tazelaar HD, et al. Five-year lung cancer screening experience: CT appearance, growth rate, location, and histologic features of 61 lung cancers. Radiology. 2007; 242: 555-562.
30. Swensen SJ, Silverstein MD, Ilstrup DM, Schleck CD, Edell ES. The probability of malignancy in solitary pulmonary nodules. Application to small radiologically indeterminate nodules. Arch Intern Med. 1997; 157: 849-855.
31. Perandini S, Soardi G, Motton M, Oliboni E, Zantedeschi L, Montemezzi S. Distribution of Solid Solitary Pulmonary Nodules within the Lungs on Computed Tomography: A Review of 208 Consecutive Lesions of Biopsy-Proven Nature. Pol J Radiol. 2016; 81, 146-151.
32. Ohno Y, Hatabu H, Takenaka D, Higashino T, Watanabe H, Ohbayashi C, et al. CT-guided transthoracic needle aspiration biopsy of small (< or = 20 mm) solitary pulmonary nodules. AJR. Am J Roentgenol. 2003; 180: 1665-9.
33. Siegelman SS, Khouri NF, Leo FP, Fishman EK, Braverman RM, Zerhouni EA. Solitary pulmonary nodules: CT assessment. Radiology. 1986; 160: 307-312.
34. Grewal, RG, Austin, JH. CT demonstration of calcification in carcinoma of the lung, J Comput Assist Tomogr. 1994; 18: 867-871.
35. Zwirewich CV, Vedal S, Miller RR, Müller NL. Solitary pulmonary nodule: high-resolution CT radiologic-pathologic correlation. Radiology. 1991; 179: 469-76.
36. Chu ZG, Sheng B, Liu MQ, Lv FJ, Li Q, Ouyang Y. Differential Diagnosis of Solitary Pulmonary Inflammatory Lesions and Peripheral Lung Cancers with Contrast-enhanced Computed Tomography. Clinics. (Sao Paulo). 2016; 71: 555-561.
37. Nambu A, Araki T, Taguchi Y, Ozawa K, Miyata K, Miyazawa, M, et al. Focal area of ground-glass opacity and ground-glass opacity predominance on thin-section CT: discrimination between neoplastic and non-neoplastic lesions. Clin Radiol. 2005; 60: 1006-1017.
38. Balagurunathan Y, Schabath MB, Wang H, Liu Y, Gillies RJ. Quantitative Imaging features Improve Discrimination of Malignancy in Pulmonary nodules. Sci Rep. 2019;9(1):8528.
39. Lu H, Mu W, Balagurunathan Y, Qi J, Abdalah MA, Garcia AL, et al. Multi-window CT based Radiomic signatures in differentiating indolent versus aggressive lung cancers in the National Lung Screening Trial: a retrospective study. Cancer Imaging. 2019;19(1):45.

Figures

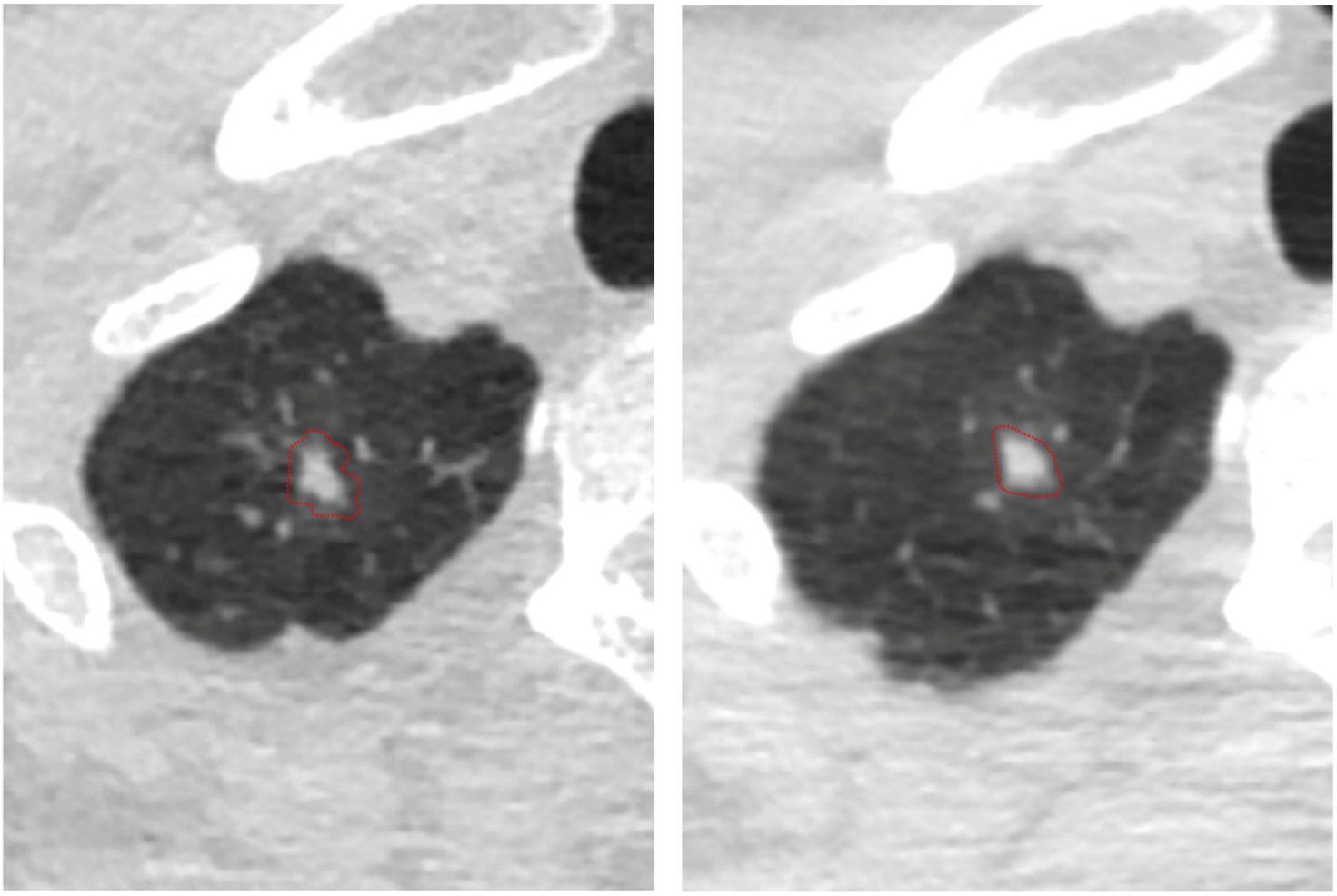

Figure 1

(A-C) CT images of lung adenocarcinoma. (A) CT image shows an irregular solid nodule (6 × 4 mm) with blurred margin locating in the apical segment of right upper lobe. (B) One year later, the size of this nodule (8 × 6 mm) increases and its shape and margin become more regular (triangle) and clearer than before. (C) Histopathologic analysis of the resected nodule revealed microinvasive adenocarcinoma.

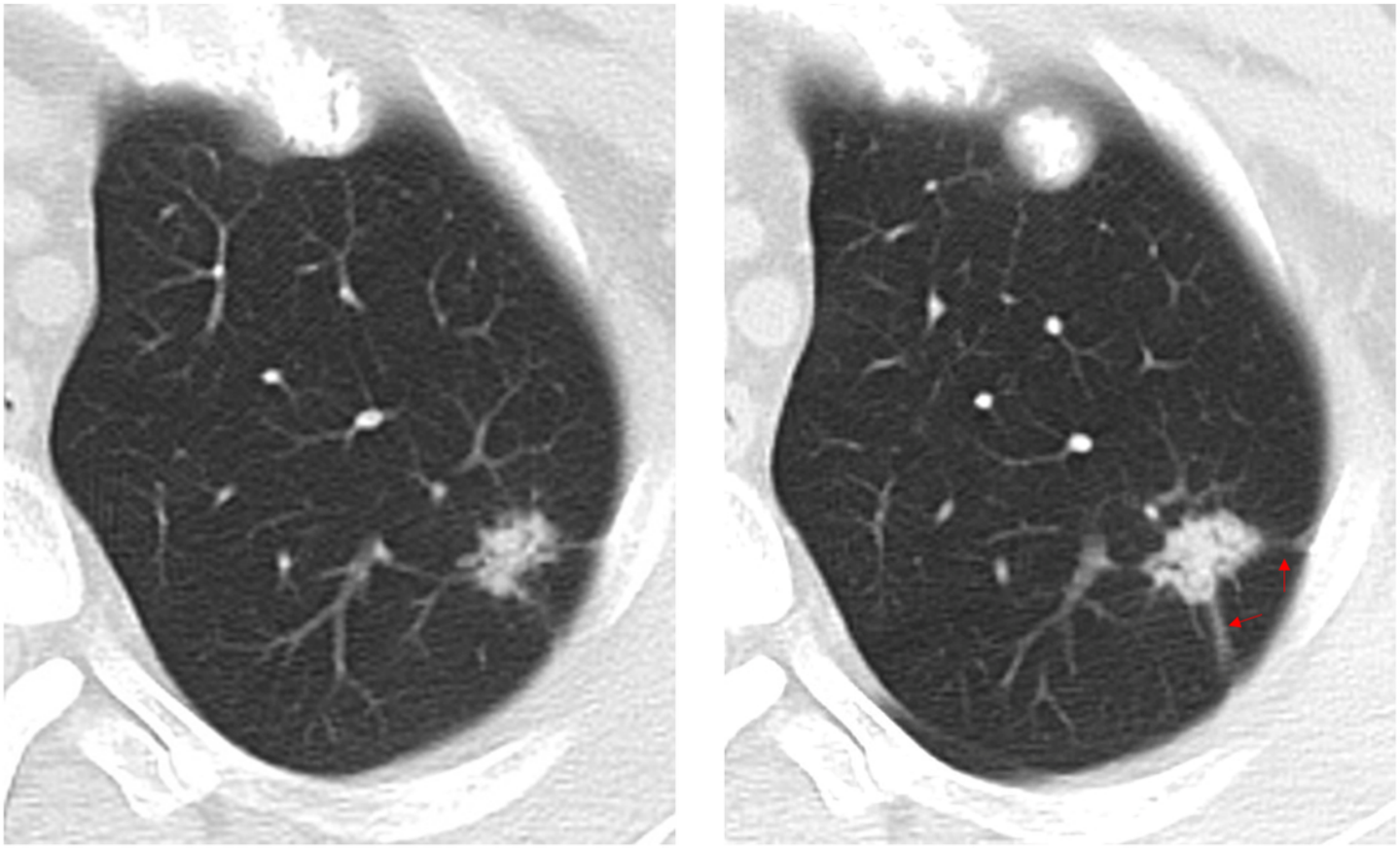

Figure 2

(A-C) CT images of lung adenocarcinoma. (A) CT image shows an irregular solid nodule (10 × 15 mm) with heterogeneous density locating in the apico-posterior segment of left upper lobe. (B) one year later, its size (14 × 16 mm) and density increased, and the tumor-lung interface is clearer and spiculation (red arrows) is more obvious than before. (C) Histopathologic analysis of the resected nodule revealed invasive adenocarcinoma.

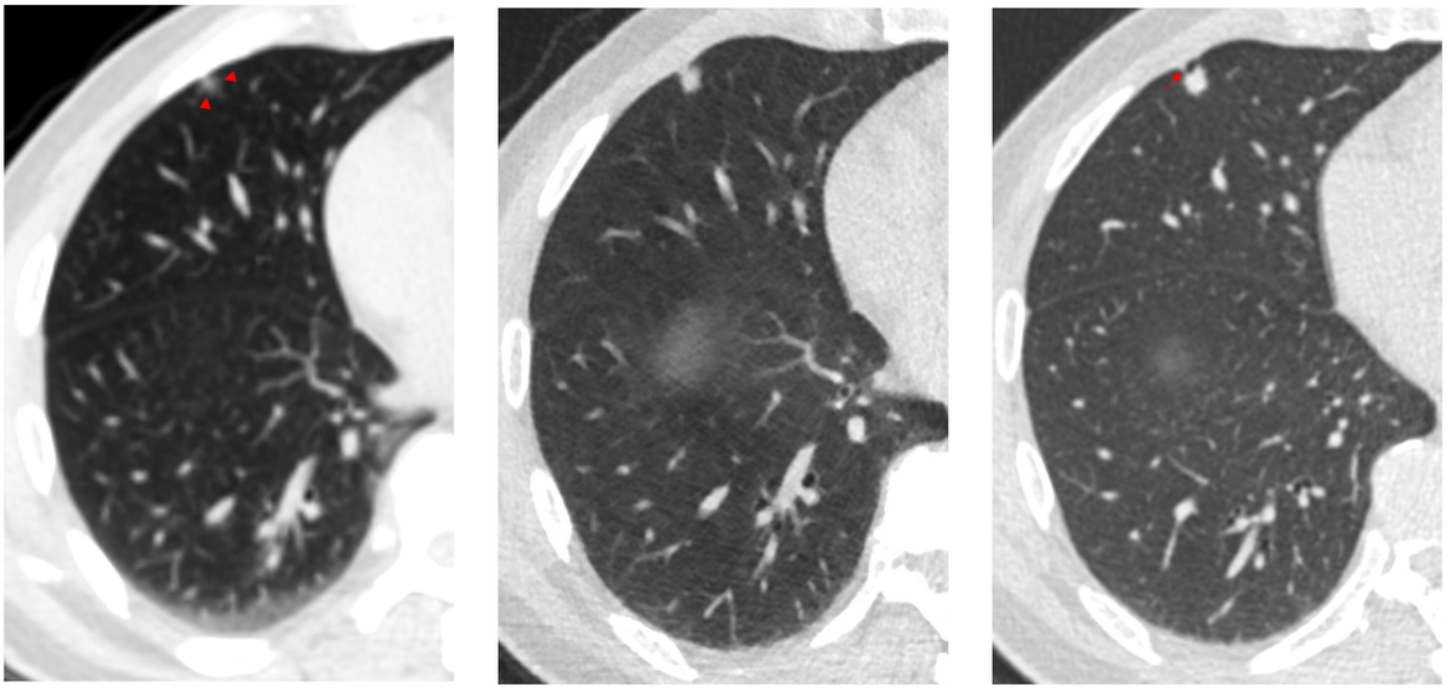

Figure 3

(A-D) CT images of lung adenocarcinoma. (A) CT image shows a nodule (7.0 × 5.0 mm) with heterogeneous density and blurred tumor-lung interface (red arrowheads) locating in the subpleural zone of right middle lobe. (B) One year and a half later, it grows a little (8.0 × 6.0 mm) but its density significantly increases. (C) Two years and a half later, its size (8.0 × 8.0 mm) slightly increased but margin becomes clearer than before. Lobulation and pleural indentation (red arrow) are obvious. (D) Histopathologic analysis of the resected nodule revealed adenocarcinoma without significant invasion.

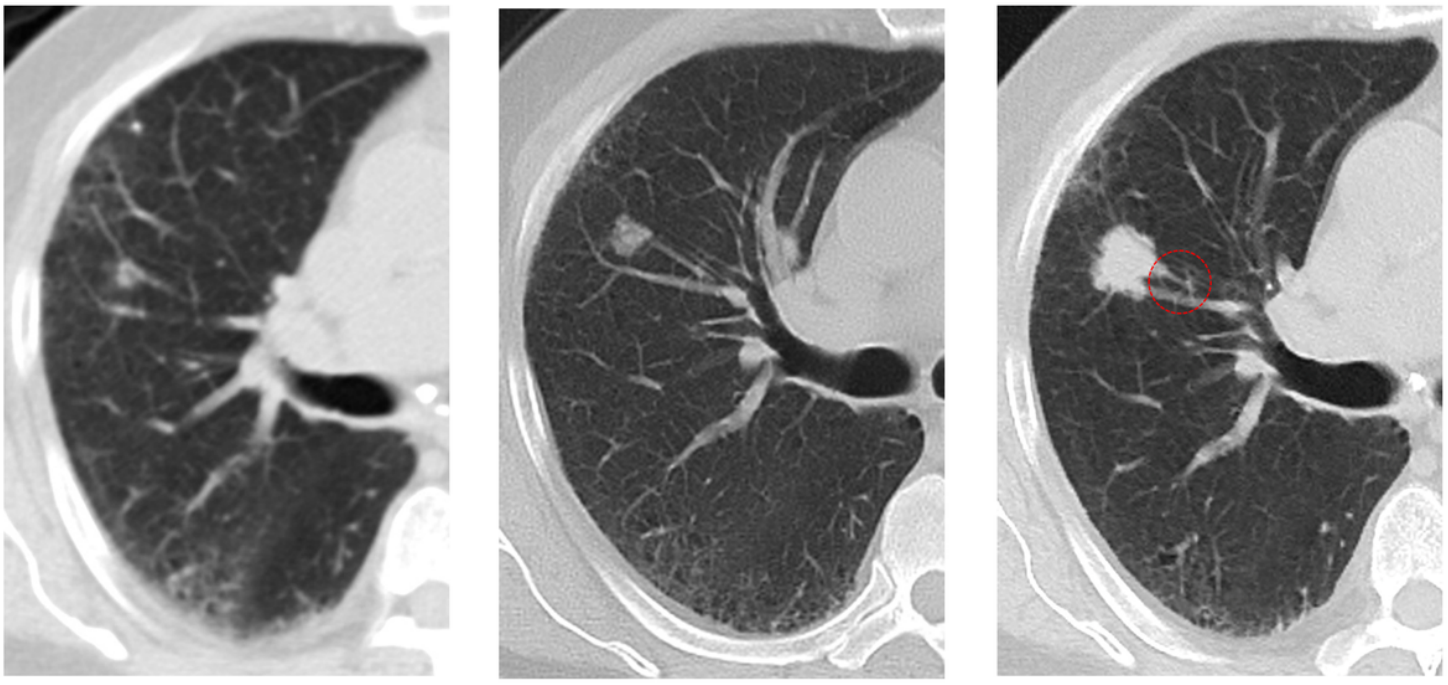

Figure 4

(A-D) CT images of lung adenocarcinoma. (A) CT image shows a small nodule (5 mm) beside vessel in the right upper lobe. (B) Eight months later, its size increases (10 ×11 mm) but its density is heterogeneous. (C) Fifteen months later, its size significantly increases (18 × 19 mm) and it has higher and more homogeneous density. Additionally, lobulation sign and peripheral vascular convergence (red circle) are positive. (D) Histopathologic analysis of the resected nodule revealed invasive adenocarcinoma.